


The notochord in Atlantic salmon (*Salmo salar* L.) undergoes profound morphological and mechanical changes during development

Harald Kryvi,¹ Iselin Rusten,¹ Per Gunnar Fjellidal,² Kari Nordvik,¹ Geir K. Totland,¹ Tine Karlsen,³ Helge Wiig³ and John H. Long Jr⁴ 

¹Department of Biology, University of Bergen, Bergen, Norway

²Institute of Marine Research, Bergen, Norway

³Institute of Biomedicine, University of Bergen, Bergen, Norway

⁴Department of Biology, Department of Cognitive Science, Vassar College, Poughkeepsie, NY, USA

Abstract

We present the development of the notochord of the Atlantic salmon (*Salmo salar* L.), from early embryo to sexually mature fish. Over the salmon's lifespan, profound morphological changes occur. Cells and gross structures of the notochord reorganize twice. In the embryo, the volume of the notochord is dominated by large, vacuolated chordocytes; each cell can be modeled as a hydrostat organized into a larger cellular-hydrostat network, structurally bound together with desmosomes. After the embryo hatches and grows into a fry, vacuolated chordocytes disappear, replaced by extracellular lacunae. The formation of mineralized, segmental chordacentra stiffens the notochord and creates intervertebral joints, where tissue strain during lateral bending is now focused. As development proceeds towards the parr stage, a process of devacuolization and intracellular filament accumulation occur, forming highly dense, non-vacuolated chordocytes. As extracellular lacunae enlarge, they are enclosed by dense filamentous chordocytes that form transverse intervertebral septa, which are connected to the intervertebral ligaments, and a longitudinal notochordal strand. In the vertebral column of pelagic adults, large vacuolated chordocytes reappear; cells of this secondary population have a volume up to 19 000 times larger than the primary vacuolated chordocytes of the early notochord. In adults the lacunae have diminished in relative size. Hydrostatic pressure within the notochord increases significantly during growth, from 525 Pa in the alevins to 11 500 Pa in adults, at a rate of increase with total body length greater than that expected by static stress similarity. Pressure and morphometric measurements were combined to estimate the stress in the extracellular material of the notochordal sheath and intervertebral ligaments and the flexural stiffness of the axial skeleton. The functional significance of the morphological changes in the axial skeleton is discussed in relation to the different developmental stages and locomotor behavior changes over the lifespan of the fish.

Key words: Atlantic salmon; axial skeleton; chordocytes; development; intervertebral joints; notochord; vertebral column.

Introduction

A key event in the origin of the chordates was the evolution of the notochord. In living vertebrates, this cylindrical axial endoskeleton is pressurized hydrostatically, giving the body passive elastic properties that serve a variety of mechanical

functions in the course of development (Adams et al. 1990; Koehl et al. 1990; Stemple, 2005; Ellis et al. 2013a,b) and during locomotion (for reviews see Koob & Long, 2000; Long, 1995; Long et al. 2011). In early life stages the notochord provides position and fate signals to the adjacent tissues along the dorso-ventral axis in the embryo, including the neural tube, somites, and endoderm (for review see Fleming et al. 2004, 2015; Corallo et al. 2015). Vertebrates evolved metameric skeletal elements – neural and haemal arches and their associated spines – that join the notochord in the median septum. While perichordal, cartilaginous 'proto-vertebrae' are present in the earliest vertebrate fossils from the Cambrian (Holland & Chen, 2001), vertebral bodies are conspicuously absent from the other jawless fishes of the Paleozoic, leaving the notochord as the

Correspondence

John H. Long Jr, Department of Biology, Department of Cognitive Science, Vassar College, Poughkeepsie, NY 12601, USA.

E: jolong@vassar.edu

The copyright line for this article was changed on 10 August 2017 after original online publication.

Accepted for publication 4 July 2017

Article published online 8 August 2017

primary axial skeleton in large adults that appear to be active swimmers (Janvier, 1996). When vertebral bodies do evolve and fuse with the neural and haemal arches, they do so convergently, with at least three independent origins of centra in chondrichthyans, actinopterygians, and tetrapods (Koob & Long, 2000). In teleosts the notochord and surrounding vertebrae compose the primary part of the axial skeleton, which also includes ribs and intramuscular bones (Schmitz, 1995; Janvier, 1996; Grotmol et al. 2003; Hall, 2005).

The embryonic notochord consists of extracellular connective tissue fibers (collagen II) forming a sheath that creates a cylindrical chamber filled with cells of two types: (i) an outer epithelial-like layer of chordoblasts that secrete the sheath and (ii) an inner cell layer of chordocytes that contain large fluid-filled vacuoles. Work on a range of vertebrates and models demonstrates that the pressure exerted by the inflation of the vacuoles on the notochord sheath endows the notochord with a portion of its characteristic flexural stiffness (Koehl et al. 2000; Grotmol et al. 2003, 2006; Long et al. 2006a,b; Sagstad et al. 2011; Corallo et al. 2015). In the earliest life history stages, the notochord is the sole component of the axial skeleton (Janvier, 1996; Glickman et al. 2003; Nelson, 2006). Later, during development of the vertebral column in teleosts, the notochord is present in three different structures: (i) the internal intervertebral ligaments, formed from the notochordal sheath, (ii) the chordacentra, formed within the notochordal sheath, and (iii) the internal components of the intervertebral capsule, formed by chordocytes (Symmons, 1979).

In Atlantic salmon, *Salmo salar* L., vertebrae form as compound structures, initially as neural and haemal arches derived from the somites (Nordvik et al. 2005; Witten et al. 2005; Grotmol et al. 2006; Wang et al. 2013, 2014; Kaneko et al. 2016). Shortly thereafter, the first elements of the vertebral bodies mineralize as segmented ring-shaped chordacentra inside the notochordal sheath. These chordacentra are connected to the arches via the formation of the autocentrum and arcocentrum, a process leading to the subsequent formation of mature segmented vertebrae (Grotmol et al. 2003, 2005, 2006; Nordvik et al. 2005; Sagstad et al. 2011; Bension-Brito et al. 2012; Wang et al. 2013). As development progresses, sclerotomes deposit bone on the surface of the chordacentra, increasing their length and diameter and, in so doing, creating the amphicoelous structure characteristic of teleostean centra (Grotmol et al. 2003; Fleming et al. 2004).

In terms of mechanical function, the most important property of the axial skeleton appears to be its flexural stiffness in lateral bending (Koehl et al. 1990; Koob & Long, 2000). Flexural stiffness, EI (in units of Nm^2), is a combination of two properties: (i) E , Young's modulus (in Nm^{-2} or Pa), is a material property independent of the size and shape of the structure, and (ii) I , the second moment of area (in m^4), is a geometric property that accounts for the distribution of material relative to the neutral axis of bending.

The combined EI is defined as the proportionality constant between an applied bending moment, M (in Nm), and the resulting curvature, κ (in m^{-1}) of the structure. Thus EI is a first approximation of the intuitive notion of 'stiffness', the relationship between the forces acting on a structure and how that structure changes shape in response.

In the notochord of adult Atlantic hagfish, *Myxine glutinosa*, EI is controlled, in part, by the vacuolated chordocytes; when vacuolated chordocytes are replaced with the same volume of extracellular fluid, EI of the notochord decreases significantly (Long et al. 2006a). Furthermore, the notochord of hagfish is osmotically active, with different concentrations of external fluid increasing or decreasing the notochord EI relative to that of the control (Sinwell et al. 1999). Finally, those changes in EI are caused by changes in the hydrostatic pressure, P , inside the notochord (Czuwala et al. 2000). This relationship between EI and P was verified in a mechanical model of a notochord (Koehl et al. 2000).

Given the functional connections between chordocytes, P , and EI , it is reasonable to predict that P and EI will change over the course of development as the tissues of the notochord, including the chordocytes, change. In salmon, during early developmental stages, P may increase by the inflation of fluid-filled intracellular vacuoles in the chordocytes, which are confined inside the notochordal sheath, composed primarily of collagen II and elastin (Grotmol et al. 2006). In salmon, this morphology lasts until about 100 day-degrees (d°) before the end of the alevin stage, the first stage outside of the egg (Fig. 1), characterized by the presence of a yolk sac and an infaunal habitat. With the appearance of the chordacentra, and the rest of the vertebral bodies, the overall stiffness of the column should increase, as predicted by adding artificial centra to the notochord of hagfish (Long et al. 1998). With bone increasing the E of the vertebral column EI in salmon, the notochord, now partially segmented into intervertebral capsules, modulates bending at the intervertebral joints.

In other teleosts, during the development of the vertebral column the notochord tissues reorganize, with the appearance of non-vacuolated chordocytes and extracellular lacunae (Symmons, 1979; Schmitz, 1995; Kvellstad et al. 2000; Nowroozi et al. 2012). The morphogenesis and functional significance of these changes are not well understood. In adult perch, *Perca fluvescens*, the intervertebral joints are chambers, formed by opposing amphicoelous centra that contain complex structures derived from the notochord, including chordocytes and extracellular lacunae (Schmitz, 1995, 1998).

The Atlantic salmon is an inviting species for developmental studies. The eggs and larvae are relatively large, and morphogenesis is adapted to cold river water and thus is relatively slow. The behavioral and ecological demands of the environment change a number of times over the complex, anadromous life cycle of a salmon (Fig. 1): the embryo resides in the egg; the hatched larvae, called alevin, live in the gravel bed and feed off their attached yolk sac; without

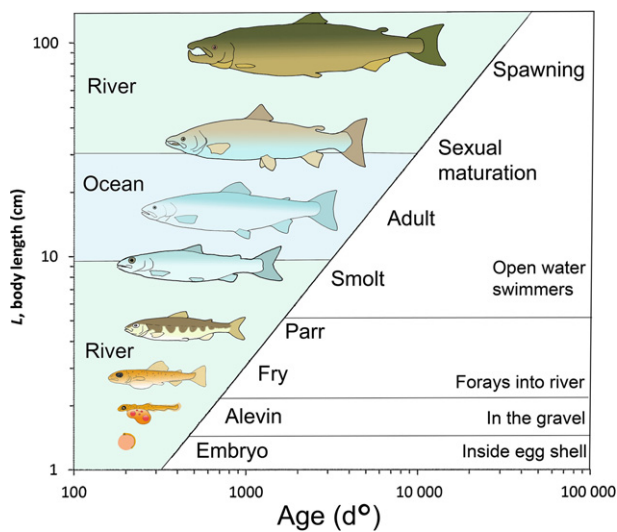


Fig. 1 Integrated life history, development, and locomotor behavior of the Atlantic salmon, showing all stages examined in this study. As the anadromous life cycle unfolds, early body movements in the embryo change to interactions with gravel in the early hatching, known as an alevin, which retains a yolk sac. The fry is the first stage to exhibit regular swimming movements; the older, larger parr swim more regularly in the water column of the river before metamorphosing into ocean-going smolt. After maturing in the pelagic marine habitat for some years, adults return to their natal river to spawn. Developmental age is measured in day-degrees (d°), a standard metric that recognizes that the rate of development is proportional to temperature. Body length is total length (cm) estimated from d° using Hansen & Møller (1985).

a yolk sac, larvae are called fry and begin to swim and forage in the water column; parr are juveniles who swim and feed primarily in the water column of the river; after 1–6 years in the river, parr may become smolts, who adjust physiologically to life in seawater and migrate to the ocean; adults live in the ocean for 1–3 years before returning to their natal river to spawn.

Because the life cycle of salmon requires different functions of the notochord – helping elongate the embryo, moving the body against and within gravel substrate, and participating in the undulatory flexures associated with swimming in rivers and long-distance migration – we predict that its structure will vary in concert. In the present study we focus on the changes in the notochord with regard to overall morphology, cell structure and differentiation, hydrostatic pressure, and flexural stiffness. The study ranges in scope from the early, unsegmented notochord of the embryo to the vertebral column of the adult.

Materials and methods

Fish and rearing conditions

Eggs, larvae, juveniles, smolt, and adult Atlantic salmon (*Salmo salar* L.) were supplied from local hatcheries and fish farm facilities in

western Norway. The various stages were kept in flow-through systems. Developmental stages are classified by day-degrees (d°), the sum of mean ambient temperature ($^\circ\text{C}$) for each day of development. Eggs and fish from 100 d° up to sexually mature fish were studied in a number of stages. For the embryonic stages, water temperatures were kept at 8.0 $^\circ\text{C}$. Embryos hatched at approximately 500 d° , at which time water temperature was raised to 8.5 $^\circ\text{C}$ and held there until the alevin had consumed their yolk sacs, at approximately 850 d° . At that point, fry were fed commercial dry feed *ad libitum* and the water temperature was raised to 15.0 $^\circ\text{C}$ over a 2-day period.

For the morphological studies, fish were examined at approximately 50- d° intervals starting at 110 d° , the first time at which notochords are present, until 1500 d° . Thereafter, fish begin to vary in size by age, and total body length, L , is a more convenient parameter for characterizing development. We converted d° to L using linear growth data from Hansen & Møller (1985), where $L = 16$ mm at hatching (equivalent to 500 d° in the present study) and $L = 26$ mm, where the yolk sac has disappeared (850 d° in this study). At any given stage, from 2–10 fish were examined.

All procedures were conducted at the University of Bergen, Norway, according to government guidelines (Norwegian Food Safety Authority) at the time, prior to changes of 1 July 2015. Before the preparative procedures, embryos, larvae, and smolt were anesthetized with 5% benzocaine dissolved in water; the spinal cord was then severed posterior to the cranium. Adults were killed with a blow to the head. For morphological studies, the precaudal and caudal portions of the vertebral column, ventral to the dorsal fin and ventral to the adipose fin, respectively, were examined. Precaudal and caudal were defined according to Kacem et al. (1998).

Light microscopy

For light microscopy, specimens for methacrylate embedding were fixed by immersion in a mixture of 10 mL 10% formaldehyde (fresh from paraformaldehyde), 10 mL 25% glutaraldehyde, 20 mL 0.2 M cacodylate buffer and 60 mL phosphate-buffered saline (PBS) with pH adjusted to 7.35. At 1000 d° and older, specimens were decalcified in buffered formic acid for 2–7 days, depending on size. The decalcified specimens were rinsed in PBS and dehydrated in ethanol (50, 70, and 96%) and embedded in Technovit 7100 (Heraeus Kulzer GmbH, Hanau, Germany). Sections (2 μm) were stained with 1% toluidine blue (Merck, Darmstadt, Germany), dried and mounted with Mountex™ (Hostolab Products, Spånga AB, Sweden). Digital micrographs were acquired with a ProgRes C14 camera (Jenoptik GmbH, Jena, Germany) on an Olympus Vanox AHB3 microscope employing both bright field and DIC optics (Olympus, Tokyo, Japan), and processed using Adobe PHOTOSHOP 7.0 (Adobe Systems, San Jose, CA, USA). To study adults, decalcified specimens were cut longitudinally with a sharp knife, stained with 1% methylene blue, covered with a thin glass plate, and photographed. Paraffin sections were stained for elastin according to Verhoeff as described in Nordvik et al. (2005).

Electron microscopy

For transmission electron microscopy (TEM), specimens were fixed and decalcified following the same procedure as the tissues embedded in methacrylate. They were then rinsed in PBS and dH_2O , before post-fixation in 1% OsO_4 , dehydrated in ethanol (70, 90, and 100%), and embedded in Epon 812 (Fluka Chemie AG, Buchs,

Switzerland). Ultrathin sections (50 nm) were placed on grids, contrasted with uranyl acetate and lead citrate, and viewed in a Jeol 1011 TEM.

For scanning electron microscopy (SEM), the specimens were fixed according to the same procedure as for light microscopy. Specimens were carefully sectioned with razor blades, rinsed in PBS, postfixed in 1% OsO₄, and rinsed in dH₂O. All specimens were then dehydrated in an acetone series (50, 70, 90, and 100%), dried to critical point, coated with gold-palladium and studied in a Zeiss Supra 55VP field emission SEM.

Morphometric measurements

The size of chordocytes was measured at 11 developmental stages: 158 d^o, 232 d^o, 350 d^o, 458 d^o, 564 d^o, 606 d^o, 680 d^o, 20 cm *L*, 30 cm *L*, 60 cm *L*, and 100 cm *L*. From single 2- μ m-thick sections of scaled two-dimensional light microscopy images, the circumference of each chordocyte was manually digitized and *A*, cross-sectional area (mm²), of the chordocyte was calculated (LEICA APPLICATION SUITE, version 3). We measured at least eight cells in each section. To account for the fact that many cells were not sectioned at their mid-point, only the largest chordocytes in that section were measured. A total of 516 chordocytes from 24 different individuals were measured.

Measurements of the notochord and vertebral column were also taken from light microscopy images. The following parameters were measured: diameter of the notochord or the vertebral column at the intervertebral joint; thickness, *t*, of the notochordal sheaths or the intervertebral ligaments at the intervertebral joint. In addition, the areal fractions of vacuolated cells and lacunae were measured in notochords and vertebral columns. This was done in the mid-sagittal plane using a morphometric grid to tally the area occupied by the different structures relative to the total area sampled.

Measurement of the hydrostatic pressure

Hydrostatic pressure was measured in notochords of four different life history stages: (i) alevin, (700 d^o) three individuals; (ii) fry (1000 d^o), four individuals; (iii) smolts (*L* = 20 cm), five individuals; and (iv) adults (*L* = 50 cm), five individuals. In the smolts and adults, precaudal and caudal intervertebral joints were measured. Precaudal and caudal were defined according to Kacem et al. (1998). Up to five measurements in each site were taken.

To measure the hydrostatic pressure in the lumen of the notochord, two different set-ups were used depending on the size of the fish. For larvae of age 700 and 1000 d^o, a micropuncture technique was used. The interstitial fluid pressure was measured with sharpened glass capillaries (diameter of 4–7 μ m) connected to a servo-controlled counter-pressure system (for details see Wiig et al. 1981) and a pressure transducer (model 1280C; Hewlett-Packard, Palo Alto, CA, USA). The glass capillaries were filled with hypertonic saline solution (0.5 M, colored with Evans Blue) to visualize the tip. A zero reference pressure measurement was performed within a cup of isotonic saline at the height of the puncture site before making the pressure measurement in the notochord. Acceptable measurements were those for which the following could be validated: (i) the pipette was freely communicating with the surrounding tissue, (ii) the feedback gain could be increased, and (iii) the zero reference pressure was the same before and after the measurement. The duration of each micropuncture measurement was 60 s and

output from the transducer was recorded on a Gilson chart recorder. This micropuncture technique was only suitable for the earliest stages, since pipette tips break when attempting to penetrate the thicker tissues of larger animals.

For the larger fish, the wick-in-needle method was employed (Fadnes et al. 1977). A standard 23-gauge needle, with a side hole 2–4 mm long, was inserted into the notochord. The needle was filled with nylon floss and isotonic saline and connected through a catheter to a transducer dome and a pressure transducer (model SensoNor, Horten, Norway). The fluid communication between the notochord and the measurement system was confirmed by compression and decompression of the catheter, which caused a transient rise and fall in pressure, respectively.

Because of the large size of the needle, the wick-in-needle method is more traumatic to the tissue than the micropuncture technique. The needle was inserted through the intervertebral ligaments into the intervertebral capsule. By introducing its volume into the hydrostatic chamber, the needle must increase the pressure within the hydrostatic chamber; the degree to which the pressure changes is unknown because we lack a non-invasive means of measuring pressure before the insertion of the needle. For the 20-cm *L* smolts, the needle was inserted obliquely to avoid the tissue of the septum and to have its tip enter the fluid of the extracellular lacunae. For the 50-cm *L* adults, which have very small lacunae, the tip of the needle enters the large vacuolated chordocytes within the chamber of the intervertebral joint. The duration of each measurement was between 30 and 120 s, and output from the transducer was recorded on a Gilson chart recorder.

To determine the mechanical isolation of the intervertebral capsules in the vertebral columns, we injected fluid into joints adjacent to the capsule that contained the needle connected to the pressure transducer.

Model of stress and stiffness

Using Laplace's law, hydrostatic pressure measurements were combined with morphometry to calculate axial stress, σ (N m⁻²), in the sheath of the notochord or intervertebral ligaments (for a review see Quillin, 1998):

$$\sigma = \frac{Pr}{2t}, \quad (1)$$

where *P* (in Pa) is the hydrostatic pressure, *r* (mm) is the radius of the notochord or intervertebral joint, and *t* (mm) is the thickness of the notochordal sheath or intervertebral ligaments. Since *P* creates σ when the notochord is straight and at rest, we can model the effect as a 'pre-stressing' of the notochord, imposing on it a non-zero flexural stiffness, *El*. Prior to bending, the initial material stiffness, *E* (in Pa), can be estimated using *P* (in Pa). The second moment of area, *I* (in m⁴), is calculated for the notochordal sheaths as follows, assuming a circular cross-section:

$$I = \frac{\pi}{4}(r^4 - (r - t)^4), \quad (2)$$

where *r* (mm) is the outer radius of the notochord or intervertebral joint and *t* (mm) is the thickness of the notochordal sheath or intervertebral ligaments. Note that when used to calculate *El*, *I* is converted to units of m.

The use of the simple hydrostatic model (Eq. 1) depends on a number of assumptions, including a ratio of r to t that is greater than 10 (i.e. thin walls), a non-tapering right circular cylinder, and a continuous, non-chambered vessel. Since these assumptions are often violated in real biological hydrostats, we use this model only as a first approximation of the relative changes in σ in the notochordal sheaths or intervertebral ligaments as has been done for the notochords of *Xenopus* embryos (Adams et al. 1990).

By definition, a hydrostatic skeleton bears tensile loads in its walls and compressive loads in its internal fluid. But bone can bear both tension and compression and thus needs no pressurized fluid for support. Thus, if the intervertebral joints of the vertebral column have a positive hydrostatic pressure, the vertebral column can be modeled as a hybrid skeleton, with a series of pressurized hydrostatic chambers alternating with bony vertebrae that restrict bending to the joints. Further complications arise when one considers that vacuolated chordocytes can each be modeled as a hydrostat, and the population of those cells, in turn, modeled as a cellular-hydrostat network that gives solid-like properties to the notochord (Long et al. 2006a).

Scaling

The developmental series of A , r , t , l , P , and σ allows us to test scaling hypotheses in salmon. Geometric similarity predicts that shape will remain the same with increasing body size, also known as isometric growth. Using L as the size measurement, geometric similarity makes the following prediction for linear measurements r or t :

$$r, t \propto L^1. \quad (3)$$

The ratio of t and r , t/r , important for understanding the relation between P and σ (Eq. 1), yields the following expectation under geometric similarity:

$$\frac{t}{r} \propto L^0 \quad (4)$$

For features measured in two dimensions, such as the area of the chordocytes, A , geometric similarity makes the following prediction:

$$A \propto L^2. \quad (5)$$

Because l contains four linear dimensions (Eq. 2), it is expected to scale as follows under geometric similarity:

$$l \propto L^4. \quad (6)$$

Static stress similarity (Quillin, 1998) predicts that σ will remain constant with changes in body size:

$$\sigma \propto L^0. \quad (7)$$

To create a scaling model for stress, one must understand the source of the P that creates the σ . In earthworms (Quillin, 1998), the P is assumed to come from muscle. But that is not the case in notochords, which have been shown to be osmotically active in *Xenopus* embryos (Adams et al. 1990) and adult hagfish, *Myxine glutinosa* (Czuwala et al. 2000). Osmotic pressure, governed by the

ideal gas law, depends on the relative concentration of solutes in the extracellular fluid inside and outside of the notochord. At equilibrium we have no *a priori* reason for these concentrations to vary with body size, hence the pressure and the stress should remain constant with changes in L .

Results

Skeletal elements

In the embryo, the first skeletal elements to form, at 370 d^o, are lepidotrichia in the dorsal and anal fin, along with hypurals of the caudal fin (Fig. 2). The first vertebral elements to appear are the neural and hemal arches, which, at 400 d^o, appear first near the anal fin and then are found throughout the column by 450 d^o. Lateral ribs and intramuscular bones appear cranially at 560 d^o and are complete axially by 640 d^o. Vertebral chordacentra are the last skeletal elements to appear, at 640 d^o, forming intervertebral joints throughout most of the column by 750 d^o.

The unsegmented notochord

The early notochord (from 110 d^o) is a rod composed of chordocytes surrounded by a thin extracellular sheath, likely a basal lamina (Fig. 3A). In the early stages, up to 200 d^o, the chordocytes have a flattened discoidal shape, with diameters initially matching that of the notochord (50 μm) and an anteroposterior length of 5–10 μm . These non-vacuolated chordocytes form a serial array of single cells that Kuntz (2004) has likened to a 'stack of coins' (Fig. 3A,B).

Concomitant with chordocyte differentiation, profound changes in notochord architecture take place. At approximately 200 d^o, a vacuolization process starts cranially to create a population of cells that we call primary vacuolated chordocytes. Numerous small vacuoles increase rapidly in size, and fuse (Fig. 3C), creating a single fluid-filled intracellular vacuole that makes up more than 95% of the cell volume at 750 d^o (Fig. 3D). The chordocytes are surrounded by a monolayer of epithelioid non-vacuolated chordoblasts, often designated the notochordal epithelium. The chordoblasts secrete the notochordal sheath, which consists mainly of collagen II fibrils and elastin (Grotmol et al. 2006). The chordoblasts range in shape from thin squamous to cylindrical, and retain their mitotic properties. By 700 d^o the vacuolated chordocytes make up the bulk of the notochord volume. The peripheral cytoplasmic rim of each vacuolated chordocyte is smooth and has a thickness of about 2 μm (Fig. 3E,F). The cells are attached to each other by numerous desmosomes, and the majority of the cytoplasmic constituents are the intermediate filaments (Fig. 3G,H). Initially, up to 600 d^o, the morphology of vacuolated chordocytes in this primary population is uniform.

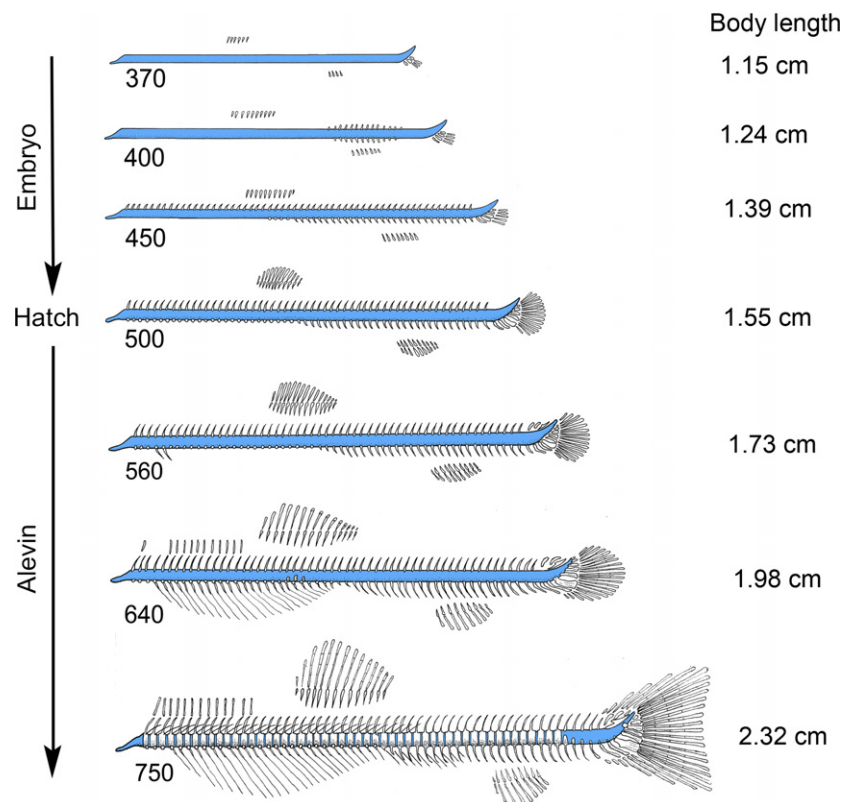


Fig. 2 From notochord to vertebral column, schematic representation. This part of the axial skeleton develops from a notochord devoid of vertebral elements, as an early embryo, to a vertebral column with neural and hemal arches and then chordacentra at the early fry stage. The first skeletal elements to appear are the hypurals in the caudal fin and radials in the dorsal and anal fins at 370 d°. The first neural and hemal arches appear at 400 d°. The first chordacentra appear at 640 d° at vertebra 27. Body length is total length (cm) estimated from d° using Hansen & Møller (1985). [Colour figure can be viewed at wileyonlinelibrary.com]

Chordocytes and the formation of chordacentra and intervertebral joints

Mineralization in the fibrous sheath commences at approximately 700 d°. Ring-shaped chordacentra form in each post-cranial body segment (Fig. 3D). The inner diameter of the chordacentrum is 420 μm , and this does not change size during development. These initial chordacentra form the narrow central canal of each mature vertebral body. As development proceeds, concentric mineralized layers are added on the exterior of each of the initial rings, with each cylindrical layer having a larger diameter and axial length. This growth pattern is responsible for the typical hourglass-like shape (amphicoelous) of the teleostean vertebrae. The notochord is thus radially symmetric with respect to the central longitudinal axis.

Until 1300 d° the notochord is filled with vacuolated chordocytes. At this stage, extracellular spaces, lacunae, start to form in concert with the forming vertebral bodies (Fig. 4A,B). By 1700 d°, each lacuna, radially symmetric about the axis of the notochord and shaped like an elongated toroid, lies in series with other lacunae, an array occupying the bulk of the notochordal volume (Fig. 4C). The

boundary of a lacuna is formed by the central notochordal strand and two intervertebral septa; both structures are composed primarily of unvacuolated chordocytes. The intervertebral septum connects peripherally with a layer of chordoblasts adjacent to the notochordal sheath, which forms the internal intervertebral ligament (Fig. 4C–E). In parr, the extracellular lacunae make up 60% of the notochordal volume.

Based on developmental series of static micrographs, we infer the following temporal dynamics in cellular morphology leading to the parr-stage notochord. The chordocytes that form the notochordal strand and the intervertebral septum rapidly accumulate intermediate filaments. In parallel, vacuolated chordocytes are confined to the intervertebral septa and near the intervertebral ligaments (Fig. 4D,E). Instead of vacuolated chordocytes, dense chordocytes are observed that characterize the parr stage (Fig. 4F–I). A stratified squamous epithelium lines the inner surface of the vertebrae (Fig. 4F). Towards the lacunae the squamous epithelial chordocytes become increasingly flattened, as thin as 0.3 μm (Fig. 4F). The irregular extensions of these cells are low, longitudinal ridges (Fig. 4G). These squamous epithelial chordocytes cover the notochordal strand and

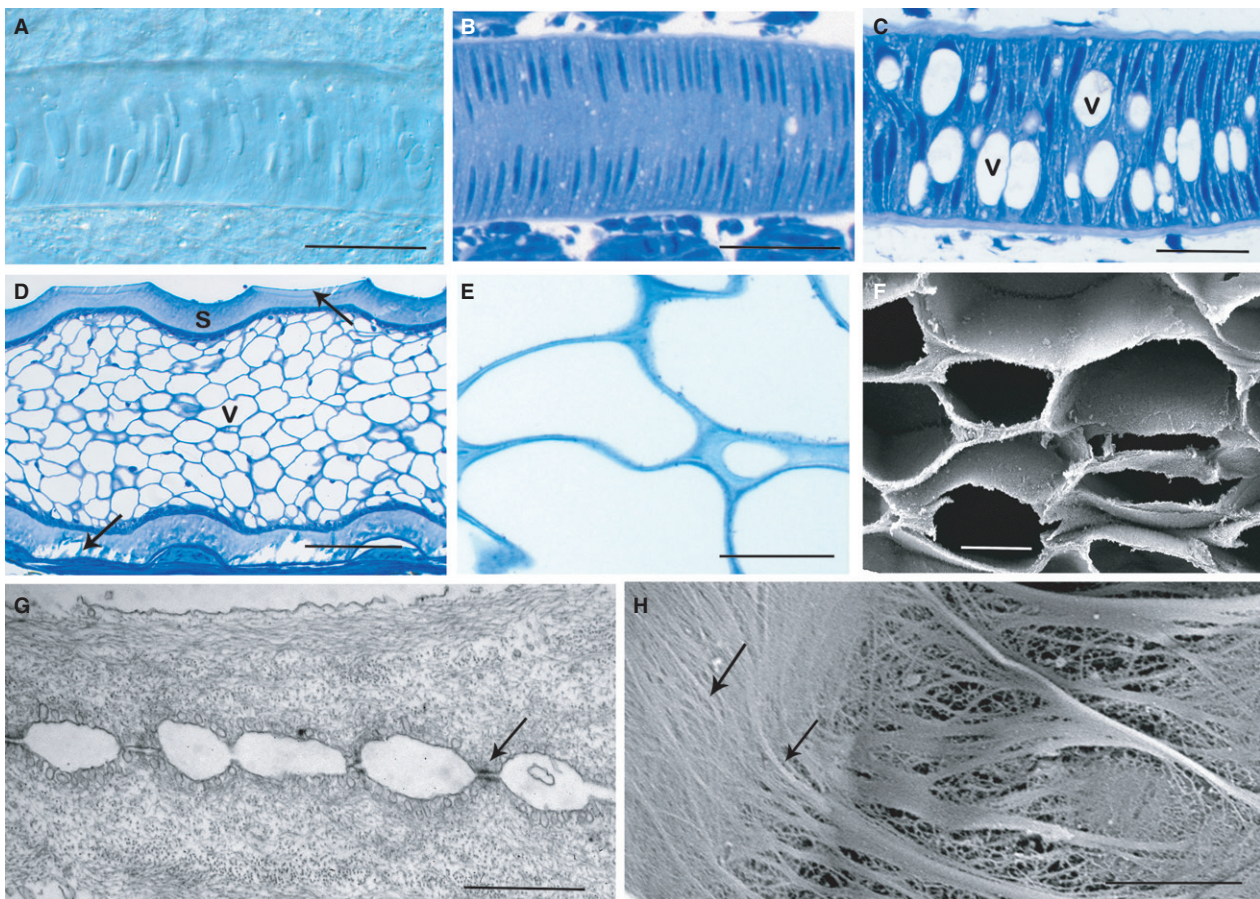


Fig. 3 Early development of the notochord as embryos grow to alevins. (A) At 150 d° each non-vacuolated chordocyte spans the diameter of the notochord and is compressed in the axial dimension, called a 'coin-stack' configuration. Nuclei are visible as ellipsoidal bodies. Whole mount, DIC, longitudinal view. Scale bar: 50 μ m. (B) By 170 d°, the chordocyte nuclei (dark stain) have moved towards the periphery and small intracellular vacuoles (white circles and ellipses) have begun to form. Technovit section stained for toluidine blue. Scale bar: 50 μ m. (C) Vacuoles (v) enlarge. Scale bar: 50 μ m. (D) By 750 d°, the intracellular vacuoles occupy most of the volume of the chordocytes, which no longer span the diameter of the notochord individually, and attain a more spherical shape. The chordocytes are surrounded by an epithelial-like layer of chordoblasts (dark layer) that secrete the notochord sheath (s); bony chordacentra (arrows) superficial to the sheath have begun to form segments. Technovit section, stained for toluidine blue. Scale bar: 100 μ m. (E) Vacuolated chordocytes, magnified, showing thin rim of cytoplasm that surrounds the large vacuoles at 750 d°. Technovit section stained for toluidine blue. Scale bar: 20 μ m. (F) Vacuolated chordocytes showing the structural network formed by the cells at 750 d°. SEM. Scale bar: 20 μ m. (G) The network of vacuolated chordocytes is characterized by desmosomes (arrow) linking cells physically accompanied by densely packed intermediate filaments in the cytoplasm at 900 d°. TEM. Scale bar: 1 μ m. (H) The intermediate filaments (arrows) form a dense intracellular network in the cytoplasm of the vacuolated chordocytes. SEM. 1000 d°. Scale bar: 2 μ m.

intervertebral septa with smooth surfaces facing and encapsulating the extracellular fluid.

Compared with early stages, the parr stage notochord is characterized by a variety of cell shapes. The chordoblasts have a smooth cell surface (see also Fig. 6). The adjacent chordocytes develop elaborate and irregular extensions, up to 4 μ m long (Fig. 4H,I), that interdigitate with those of the neighboring cells, forming an extensive surface area for robust intercellular attachment. The notochordal strand that connects the intervertebral septa (Fig. 5A–D) consists entirely of dense, low-ridged unvacuolated chordocytes. Nordvik et al. (2005) found that chordoblasts secrete the internal intervertebral ligament (Fig. 6A) and appear to

transform into a few secondary vacuolated chordocytes that remain located laterally, near the joint (Fig. 6B) at this stage. Based on common relative position, and the absence of other changes, we infer that the mature secondary vacuolated chordocytes are derived from this population of chordocytes, eventually filling the bulk of the notochord in smolts and adults (Fig. 7).

In these final stages, the extracellular space of the lacunae is gradually diminished, making up as little as 7% of the volume in sexually mature fish; the remaining volume is filled with secondary vacuolated chordocytes. The intervertebral septa and the longitudinal strand are inconspicuous in these later stages (Fig. 7C,D).

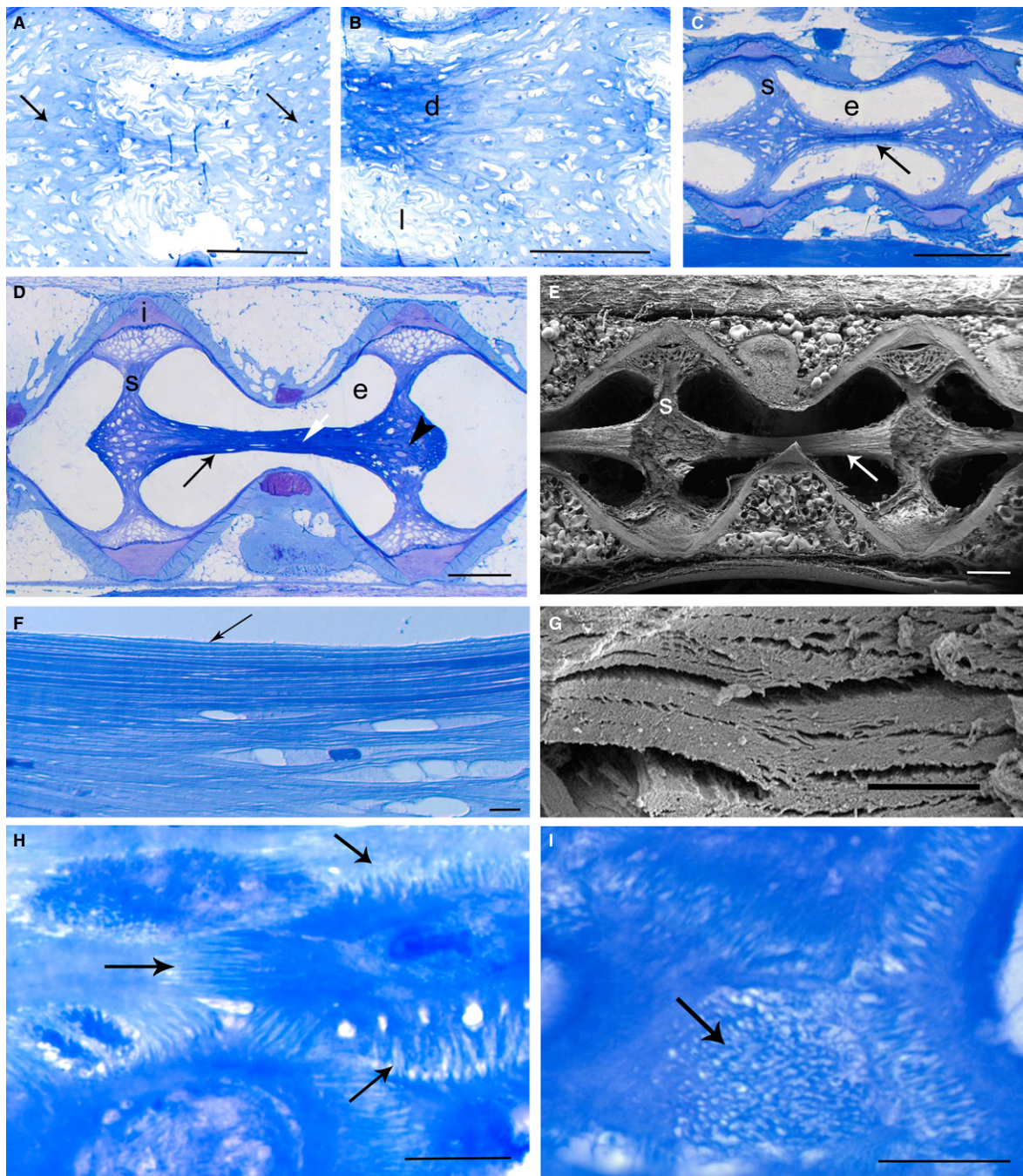


Fig. 4 Development of the notochord as alevins grow to parr. All microscopic images are Technovit sections stained for toluidine blue, except panels (E) and (G), which are SEM images. (A) At 1300 d°, alevin undergo the first stage of chondrocyte reorganization, as cells coalesce to form a segmented pattern in the future intervertebral regions (arrows), leaving more loosely organized cells with extracellular space in the mid-vertebral regions. Scale bar: 200 μm (A–C). (B) Starting at the 1500 d° stage (early parr), a dense longitudinal strand starts to form (d). (C) At 1300 d°, the chondrocytes have almost finished the reorganization. Dense assemblages of chondrocytes create segmental, transverse septa (s) and the longitudinal axial strand (arrow). These are cellular structures that delimit extracellular lacunae (e) that make up much of the volume of the notochord. (D–E) Midsagittal sections of the fully developed parr stage, with dense cells of the notochordal strand (long arrows) and septa (s), and vacuolated cells in the periphery of the transverse septa only. They connect to the intervertebral ligament (i). The short white arrow in (D) shows the location of the sections in panels (F) and (G); the black arrowhead in (D) shows location of (H) and (I). (D) Technovit section. (E) SEM image. Scale bars: 400 μm (D,E). (F–G) Parr stage. The inner surface of the notochordal strand consists of numerous layers of extremely flattened, dense chondrocytes (arrow) with irregular surface folds and slender projections. Scale bars: 5 μm (F) and 1 μm (G). (H,I) Parr stage. Densely packed chondrocytes have extensively folded surfaces, composed of irregular folds and slender projections (arrows). Notice the transverse sections of the projections, (I) The projections increase the attachment area between adjacent cells. Scale bar: 5 μm (H,I).

The secondary vacuolated chordocytes undergo rapid and dramatic growth, outstripping the size of the early vacuolated chordocytes (Fig. 8). Even though their increase in size is extreme, the population of secondary vacuolated cells does not increase as quickly as predicted by geometric similarity; the regression of chordocyte area, A , onto body length, L , yields an exponent of 1.212 (Table 1), below the value of 2 predicted by isometric growth that yields geometric similarity. The primary vacuolated chordocytes also grow allometrically, with an exponent of 1.161 (Table 1). Most striking is the discontinuous growth of the vacuolated chordocytes, producing a gap in their presence during development, a period punctuated by the formation of the extracellular lacunae (Fig. 8).

To demonstrate the large size of these chordocytes, we estimated the volume, assuming a spherical shape of cells. Using a radius, r , calculated from A , assuming circularity, we find that the largest secondary vacuolated chordocytes ($r = 0.1335$ mm in 100 cm fish) have a volume that is 19 000 times that of a chordoblast ($r \sim 5$ μm).

Over the entire life cycle of Atlantic salmon, chordocytes take on a wide variety of forms. To summarize possible developmental relationships of cells between different stages, a model of chordocyte development is proposed (Fig. 9A). Please note that this model hypothesizes temporal and spatial dynamics of cells from static micrographs; hence this model is a hypothesis that could be tested by real-time cell tracking studies (for review of methods see Meijering et al. 2012). The most important feature of this model is that multiple pathways are hypothesized to exist for the transformation of the shape and function of chordocytes. Chordocyte morphologies are extremely varied (Fig. 9B–D).

When the entire development of the notochord, from embryo to adult, is juxtaposed, dramatic changes are observed (Fig. 10). Vacuolated chordocytes appear, disappear, and reappear. Dense chordocytes, with highly folded surfaces and filled with intermediate filaments, appear and then disappear. Large extracellular lacunae appear,

dominate the fluid volume of the notochord, and then are reduced substantially in size. The notochordal sheath starts as the continuous wall of a cylindrical hydrostatic skeleton and ends up as discontinuous intervertebral ligaments connecting bony vertebrae.

Scaling of morphology, pressure, stress, and stiffness

In addition to the discontinuous patterns in notochord development, continuous growth was analyzed with simple scaling models (see Materials and Methods) that predict how structural or biomechanical features change with changes in total length, L . The linear measures of radius, r , and thickness of the notochordal sheath or intervertebral ligament, t , have an expected exponent of 1 under geometric similarity, also known as isometric growth. Both r and t conform to the prediction of geometric similarity over development, with exponents having values that are statistically different from 0 and are within the standard error for the exponent (Table 1). As would be expected by this result, the ratio of r/t has an exponent that is statistically indistinguishable from 0. The second moment of area, I , was predicted under geometric similarity to scale with L to the fourth power, as it does, within the margin of the standard error.

Throughout its development, the notochord is pressurized (Fig. 11A). Hydrostatic pressure, P , increases more than an order of magnitude from a mean of 525 ± 29.4 (\pm SE) Pa in fry (1000 d $^\circ$) to a mean of $11\,570 \pm 764.5$ (\pm SE) Pa in adults. Interestingly, the mean P in fry is less than that of the smaller alevin (700 d $^\circ$), which have a mean value of 607 ± 33.2 (\pm SE). A t -test (one-tailed, heteroscedastic variance) shows that the difference between the means is marginally significant ($P = 0.061$). The mean P in the precaudal vertebral column of adults, $10\,821 \pm 1257.6$ (\pm SE) Pa, is statistically indistinguishable from that in the caudal vertebral column, $12\,306 \pm 759.3$ (\pm SE) Pa (t -test, two-tailed, heteroscedastic variance, $P = 0.149$). Because of this

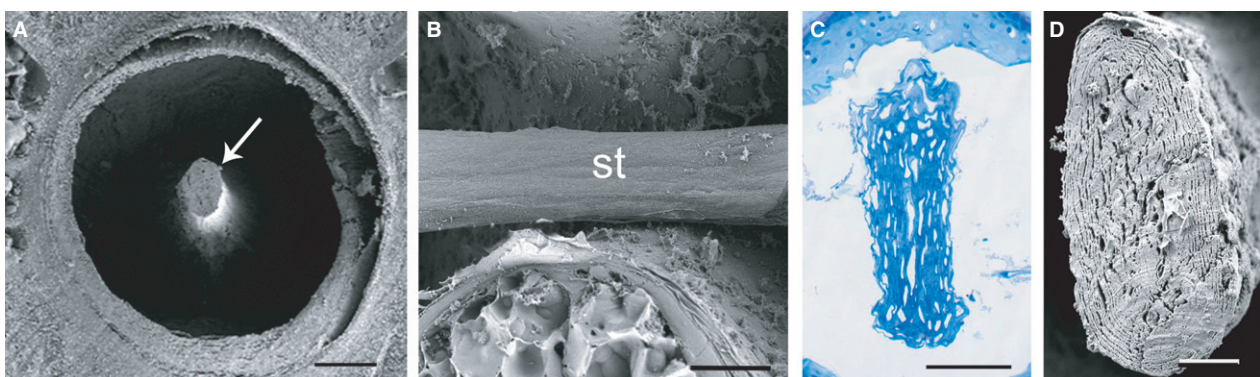


Fig. 5 The notochordal strand in the parr. (A,B,D) SEM images. (C) Light microscope image from a Technovit section stained for toluidine blue. (A) Transverse aspect of the longitudinal strand (arrow). Note the smooth surface. (B) Longitudinal aspect of the strand (st) which is composed of a roll of dense, thin cells that are seen in transverse section (C,D). Scale bars: 100 μm (A,B) and 20 μm (C,D).

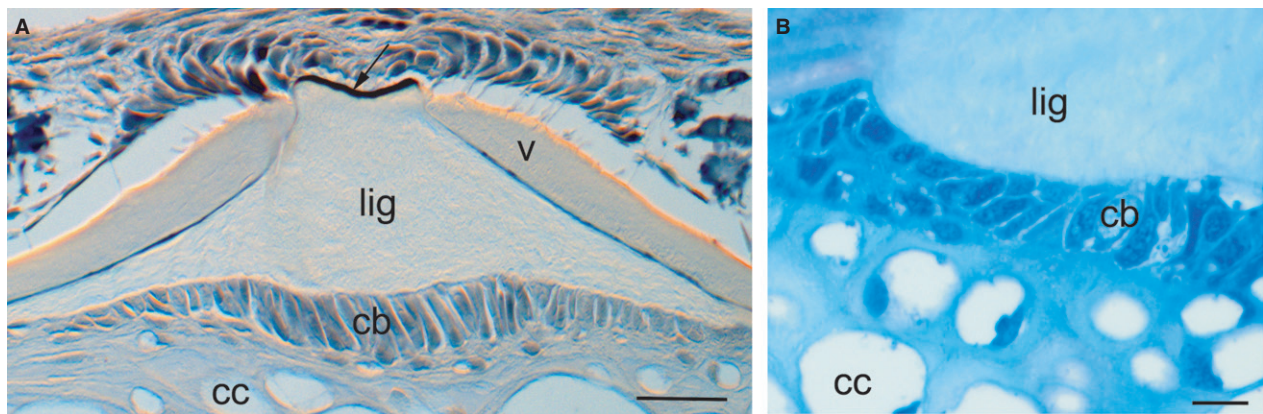


Fig. 6 Part of the intervertebral joints in the parr. Longitudinal sections. (A) Light microscopic image of a paraffin section, stained for elastin. The dark elastic ligament (arrow) covers the thick intervertebral ligament (lig), produced by the chordoblasts (cb) lying peripheral to the chordocytes (cc), and connect bony vertebrae (v). (B) In addition to producing the intervertebral ligament, the chordoblasts (cb) transform into vacuolated chordocytes (cc). Technovit section stained for toluidine blue. Scale bars: 40 μm (A) and 10 μm (B).

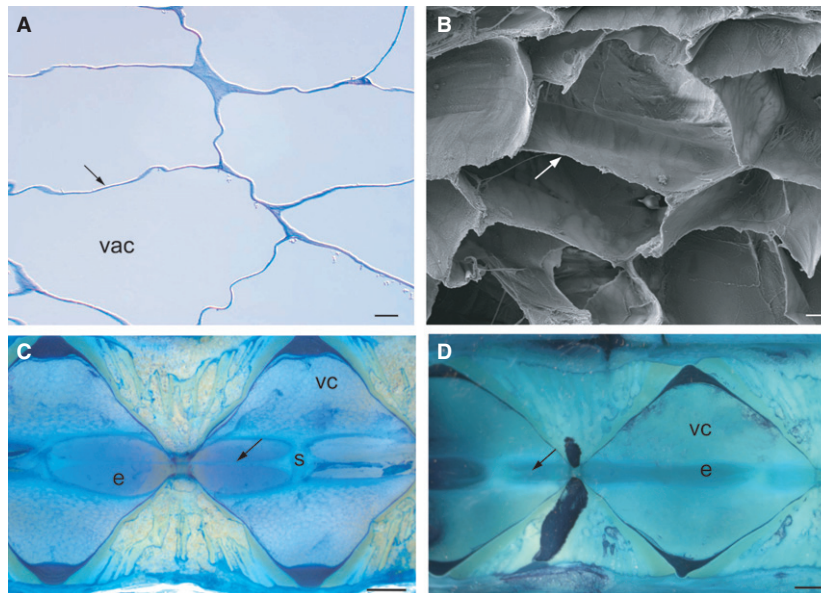


Fig. 7 The vertebral column in smolts and adults. (A–B) Large vacuolated chordocytes consist of a large fluid-filled vacuole (vac) surrounded by thin rims of cytoplasm (arrows). (A) Technovit. (B) SEM. Scale bars: 10 μm (A,B). In smolts (C) and adults (D), adjacent vertebrae form the amphicoelous intervertebral joints. Large vacuolated chordocytes (vc) are abundant, while reduced in size, relative to the parr, are the extracellular lacunae (e), the transverse septa (s), and the notochordal strand (arrow). Scale bars: 1 mm (C,D). Both (C) and (D) are gross horizontal sections stained with methylene blue.

similarity, P -values were pooled across anatomical sections for the scaling analysis. The P scaled with L with an exponent of 0.967 (Fig. 11A; Table 1) in violation of the prediction of static stress similarity and its exponent of 0. Because of the isometric scaling of r/t (Table 1), the simple hydrostatic model then predicts that with increasing P , the stress in the sheath, σ , must increase; its scaling exponent is 0.907 (Fig. 11B, Table 1). Using σ as an estimate of the prestressed resting or initial Young's modulus, E , of the notochord, the apparent flexural stiffness, EI , was calculated, yielding a scaling exponent of 4.963 (Fig. 11C, Table 1).

When we injected fluid into intervertebral joints adjacent to the joint in which pressure measurements were taken, we found pressure in the focal joint to be influenced by injection of fluid only into the two closest joints. This suggests a strong local compartmentalization of the joints into nearly separate hydrostatic chambers.

Discussion

This is the first study to describe the morphological development of the notochord in Atlantic salmon, *Salmo salar*,

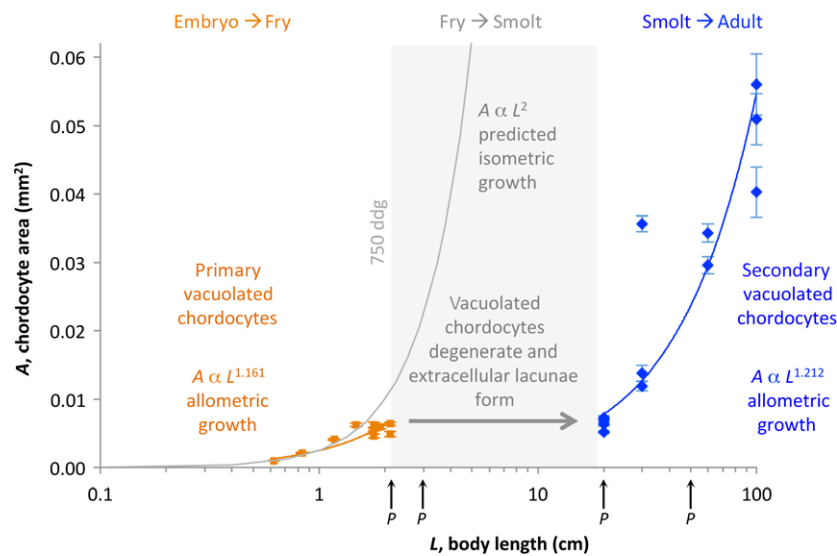


Fig. 8 Discontinuous development of vacuolated chordocytes. Vacuolated chordocytes are of two different populations (see Fig. 9). By 750 d° (left-hand side of gray shading) the growth of vacuolated chordocytes ceases; by 1300 d°, vacuolated chordocytes start to degenerate as extracellular lacunae begin to form. By 1500 d° ($L \sim 4.6$ cm) few vacuolated chordocytes remain; the notochord volume is dominated by the extracellular lacunae. Even though they differ in size, the primary (orange points and line) and secondary (blue points and line) populations of vacuolated chordocytes grow at similar rates, as shown by the exponents of their power fits (see Table 1 for complete results). Both populations of cells grow allometrically, at a rate less than that expected by isometric growth (gray solid line, exponent of 2). The four sizes at which hydrostatic pressure was measured are indicated by the black arrows (P).

Table 1 Scaling equations.

Variable	Symbol	Intercept	Exponent	SE	<i>n</i>	<i>r</i> ²	<i>P</i>
Area of primary chordocytes	A_1	0.003	1.161	0.1617	22	0.866	< 0.0001
Area of secondary chordocytes	A_2	0.000	1.212	0.1687	22	0.838	< 0.0001
Radius of notochord	<i>r</i>	0.098	1.000	0.0000	20	1.000	< 0.0001
Thickness of notochordal sheath	<i>t</i>	0.012	1.064	0.1024	20	0.857	< 0.0001
Ratio of thickness to radius of notochord	<i>t/r</i>	0.125	0.064	0.1024	20	0.021	0.5411
Second moment of area	<i>I</i>	0.000	4.056	0.0816	20	0.993	< 0.0001
Hydrostatic pressure	<i>P</i>	211.211	0.967	0.0671	17	0.933	< 0.0001
Stress in sheath	σ	846.792	0.907	0.0672	17	0.924	< 0.0001
Flexural stiffness of notochord	<i>El</i>	0.000	4.963	0.0670	17	0.997	< 0.0001

Least-squares regressions were run on log-transformed data, thus providing tests and fits of scaling equations of the form: $P = aL^b$. Intercepts and exponents given above are in this power equation form. Exponents statistically different from 0 are in bold. For A_1 and A_2 , the range of body lengths, *L*, for measured fish was from a minimum of 0.49 cm to a maximum of 100 cm. For *r*, *t*, *t/r*, and *I*, the range of *L* was from a minimum of 0.85 cm to a maximum of 100 cm. For *P*, σ , and *El*, the range of *L* was from a minimum of 2.2 cm to a maximum of 50 cm.

from embryo to adult. Over its lifespan (Fig. 1), the cells, extracellular tissues, and gross structures of the notochord reorganize twice, in dramatic fashion, from that of the embryo (Fig. 10). Initially, the volume of the notochord is dominated by large, vacuolated chordocytes. After the embryo hatches and grows into a parr, those vacuolated chordocytes disappear as extracellular lacunae form medially and chordacentra appear peripherally in the notochord cylindrical sheath. In the vertebral column of pelagic adults, vacuolated chordocytes reappear and the lacunae have diminished in relative size. These anatomically deep

developmental dynamics occur together with changes in the notochord's overlying osseous vertebral structures and the behavioural ecology of the salmon.

In early and late embryos the notochord is the primary part of the axial skeleton, a continuous cylindrical sheath of extracellular tissue encircling a lumen packed with vacuolated chordocytes (Fig. 3A–C). Upon hatching, the larval alevins, possessing an external yolk sac, are infaunal, living and locomoting in the gravel (Fig. 1). At this stage, chordacentra begin to form in the notochordal sheath (Figs 2 and 3D); these centers of mineralization create rings that are

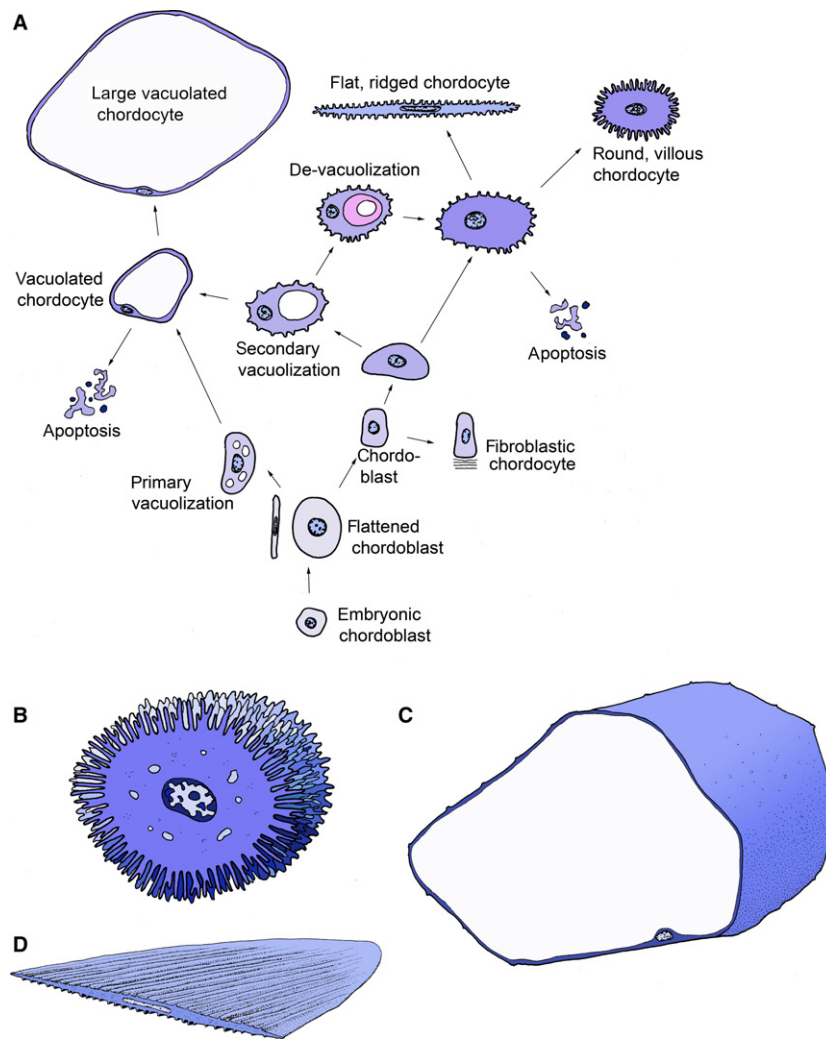


Fig. 9 Chordocyte development in salmon, schematic model. This model is a hypothesis concerning dynamic transformations that are inferred from hundreds of microscopic sections, only a small sample of which can be presented in this paper. (A) Shared, parallel, and convergent pathways. From the embryonic chordoblasts, all cells flatten before taking one of five different developmental pathways to form four differentiated types of chordocytes (names in bold). In primary vacuolization, chordoblasts enlarge as intracellular vacuoles fuse into one that grows in volume to form the large vacuolated chordocytes. These giant cells dominate the volume of the notochord in the larva until they are lost at approximately 700 d⁰. At the smolt stage of development, vacuolated chordocytes reappear secondarily from peripheral chordoblasts in register axially with the intervertebral ligaments. In this secondary pathway, vacuolated chordocytes continue to proliferate and eventually dominate the volume of the intervertebral capsule. Some vacuolated chordocytes deviate from this pathway, shrink their vacuoles (devacuolization), and form chordocytes that are either flat and ridged or round and villous. These non-vacuolated chordocytes may also differentiate directly from chordoblasts, which may also form a fourth type of differentiated chordocyte, the fibroblastic chordocyte. Three types of differentiated chordocytes differ dramatically in morphology from the progenitor chordoblasts: (B) the round, villous chordocytes have an extensively folded surface forming a carpet of slender projections; (C) the flat, dense and ridged chordocytes have the cell membrane folded into ridges rather than projections; (D) the smooth and very large vacuolated chordocytes lack both projections and folds. These three types of mature chordocytes are not drawn to scale. Note that the fourth differentiated type, the fibroblastic chordocyte, is not pictured in enlarged form.

stiffer than the adjacent non-mineralized sheath. Based on a study adding artificial plastic ring centra to the notochord of the Atlantic hagfish, *Myxine glutinosa* (Long et al. 2004), it has been proposed that ring centra create intervertebral joints that bear the bending strain that was formerly distributed along the entire notochord. For a given amount of lateral curvature imposed on these excised and altered notochords from *Myxine*, the combination of centra and

joints increases five-fold the flexural stiffness, EI , of the axial skeleton compared with that of an unsegmented notochord, *ceteris paribus*. For alevins, we predict that this increased EI of the axial skeleton will augment locomotion by allowing the 2-cm-long larva to lever its body against the gravel and move within the interstices.

As alevins lose the yolk sac and develop into fry, they face a very different and more challenging environment as they

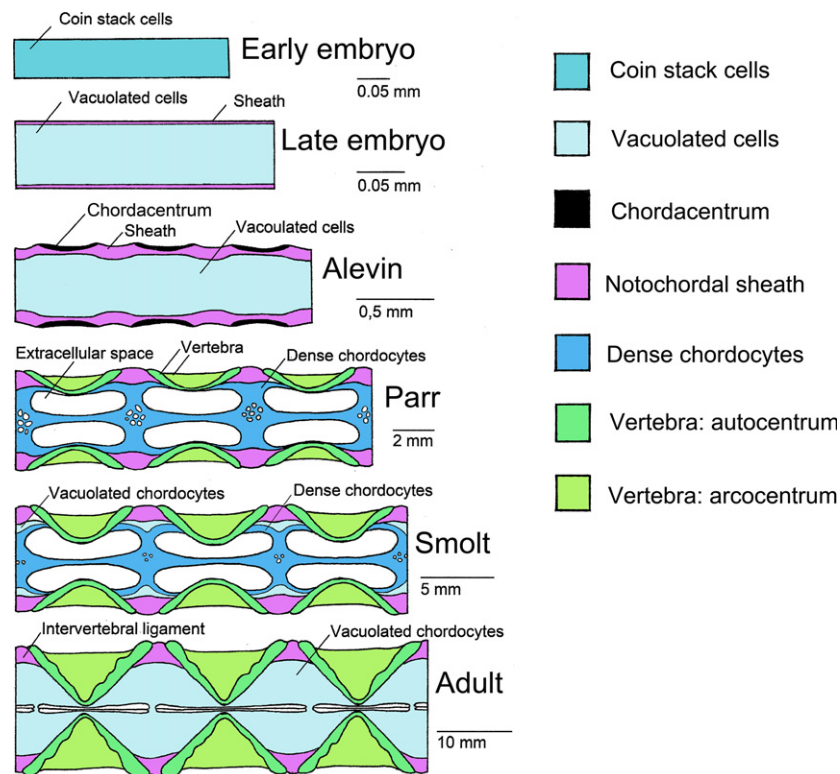


Fig. 10 Development of the larger structures of the notochord and the vertebral joints. Schematic summary of mid-sagittal sections, drawn to different scales. (A) Early embryos (up to ca. 170 d^o) have disc-shaped chondocytes, with each cell spanning the diameter of the notochord. (B) In late embryos, up to 700 d^o, the chondocytes become spherical, with no single cell spanning the notochord. (C) Newly hatched alevin have a segmented notochord with vacuolated chondocytes. (D) Parr have a notochord with prominent extracellular spaces, lacunae, and mainly dense chondocytes forming a longitudinal notochordal strand and transverse septa. (E) Smolt have a prominent longitudinal strand and transverse septa, and early formation of large vacuolated chondocytes close to the intervertebral ligaments. (F) Adults have a notochord consisting mainly of large vacuolated cells, while the strand, septa, and lacunae are insignificant.

begin forays into the water column. Simultaneously, the notochord undergoes another dramatic morphological change. The primary vacuolated chondocytes disappear, leaving extracellular, toroidal lacunae filled with fluid (Fig. 4A–D). What was originally a lumen packed completely with large chondocytes becomes a volume devoid of them and filled, instead, primarily with extracellular fluid compartmentalized into lacunae by the squamous, tightly packed non-vacuolated chondocytes forming the intervertebral septa (Fig. 10). Correlated with this morphological change, the hydrostatic pressure in the notochord drops 13% (Fig. 11A and present results). In Atlantic hagfish, vacuolated chondocytes replaced with extracellular fluid decreased the axial skeleton flexural stiffness by approximately 27–28%, all else being equal (Long et al. 2006a).

These results from salmon and hagfish are consistent with the cellular-hydrostat network (CHN) model: vacuolated chondocytes, each a small hydrostatic skeleton, are connected by desmosomes (Fig. 3G), allowing a predominately fluid volume to function as an elastic solid (Long et al. 2006a). The CHN has two important mechanical properties: (i) solid behavior – unlike a fluid, the network of cells resists both shear and torsion because of their physical

connections, creating the mechanical behavior that defines a solid; and (ii) higher hydrostatic pressure – for a given stress in the wall of a pressurized sphere or cylinder, small vessels will have higher hydrostatic pressures, since pressure is inversely proportional to the radius of the vessel (Quillin, 1998). The CHN is lost with the loss of the vacuolated chondocytes in fry. The resulting lacunae, with extracellular fluid, operate as standard hydrostatic skeletons, segmentally arrayed in series.

Lacunae dominate the notochordal volume until the smolt stage, when the fish are active swimmers in the natal river and begin to develop secondary vacuolated chondocytes (Fig. 7). During smoltification, the salmon changes from a bottom-dwelling parr to a smolt adapted to a pelagic life in the sea. The secondary chondocytes are much larger than the primary chondocytes, increasing in size as smolts develop into adults (Fig. 8). The appearance of these secondary vacuolated chondocytes is correlated with an increase in the magnitude of hydrostatic pressure by more than an order of magnitude (Fig. 11). Given that chordacentra formed in larvae (Fig. 2), this reappearance of the CHN, with higher hydrostatic pressures, is likely to be associated with increases in the flexural stiffness of the axial

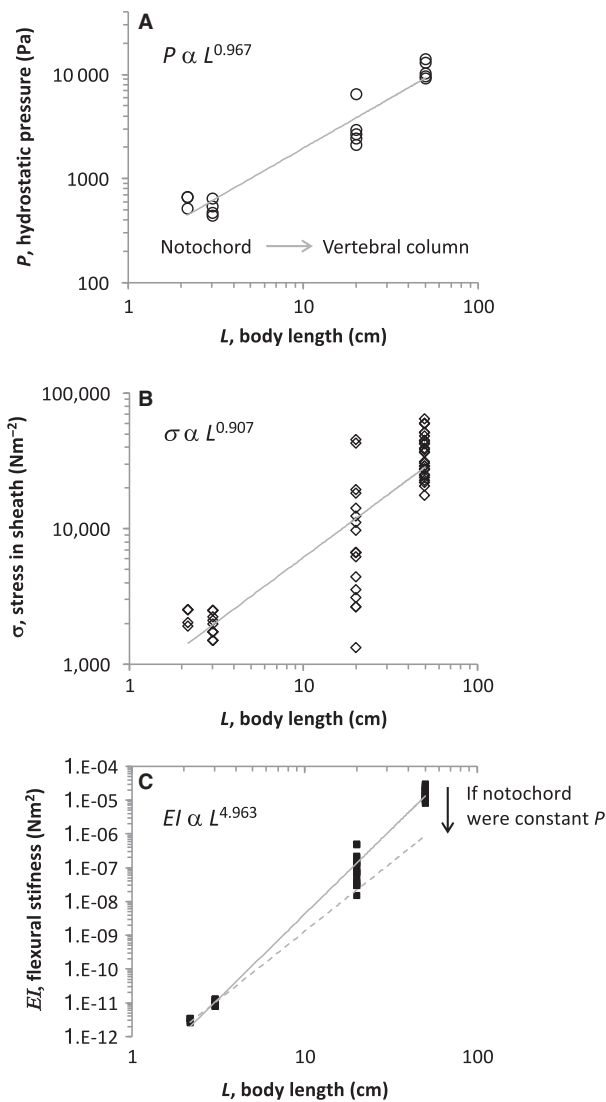


Fig. 11 Hydrostatic pressure and flexural stiffness in the developing notochord. (A) Hydrostatic pressure, P , scales with body length, L , with an exponent of nearly 1. The internal hydrostatic pressures of the notochord are an order of magnitude lower than the highest pressures found in the intervertebral joints of the vertebral column. Each point presents the mean pressure for an individual. (B) The axial stress, σ , in the notochordal sheath or intervertebral ligaments increases over nearly two orders of magnitude with increasing hydrostatic pressure as calculated by Laplace's law. The linear relation (exponent of power function approaching 1.0) indicates a constant ratio of the radius of the notochord or intervertebral joint to the thickness of the notochordal sheath or intervertebral ligaments (see Table 1). (C) The apparent initial flexural stiffness, EI , of the notochord increases seven orders of magnitude, driven by the increase in P and the increase in the second moment of area, I , of the notochord. If the hydrostatic pressure remained constant, flexural stiffness would decrease (dashed line).

skeleton. While we did not measure flexural stiffness of the axial skeleton in salmon, physical models of notochords demonstrate that increases in hydrostatic pressure increase

flexural stiffness (Koehl et al. 2000). For active undulatory swimmers, stiffer axial skeletons increase the speed of steady swimming and the acceleration of escape maneuvers, as shown in autonomous fish-like robots (Long et al. 2011). Based on this information, we predict that the axial skeleton of smolts is transforming in order to improve swimming performance.

Given that these changes in the function of the axial skeleton over the lifespan of salmon are driven, in part, by the chordocytes, it is important to examine their developmental dynamics in detail (Fig. 9). Primary vacuolated chordocytes in embryos and alevin develop from small, non-vacuolated, embryonic chordocytes that pass through a stage in which the cells are flattened and span the diameter of the notochord (Fig. 3A–C). Secondary vacuolated chordocytes in smolts and adults (Fig. 7) arise from a standing population of peripheral chordoblasts located in register axially with the intervertebral ligaments (Fig. 6B). Chordocytes from chordoblasts may bypass a vacuolization stage (Fig. 9C) and create villous chordocytes (Figs 4H–I and 9B), squamous chordocytes (Figs 4D–E and 9D), the two types of cells that form the intervertebral septa and notochordal strand (Fig. 5). The dramatic changes in chordocyte morphology and position are consistent with Shi & Keller's (1992) mediolateral intercalation behavior (MIB) hypothesis, which posits the convergence and extension of notochordal cells early in development as a driver of the formation of the vertebrate body axis. The MIB hypothesis is supported by cell-tracking studies in early notochord formation in zebrafish (Glickman et al. 2003). Moving beyond the earliest stages, our study demonstrates continued change in chordocyte morphology through development that we propose has consequences for the mechanical behavior of the notochord as swimming behavior changes throughout the salmon's lifecycle. To our knowledge, this is the first demonstration of this correlation.

In conclusion, our work on the morphology and mechanical properties of the notochord shows that what may appear at first as a simple developmental trajectory – from an unsegmented hydrostat to a segmented vertebral column – is far more complex. With fine-scale temporal resolution, we are able to show reconfigurations and changes at three structural scales. At the cellular level, chordocytes become vacuolated, reconfigure as dense epithelium, losing vacuoles, and then regain vacuoles that enlarge the cells beyond the original dimensions of the primary vacuolated chordocytes. At the tissue level, the notochordal sheath, at first continuous, becomes segmented as chordocentra mineralize within; extracellular lacunae are formed from the multicellular aggregation of dense chordocytes forming an epithelium-like boundary; vacuolated chordocytes form a cellular-hydrostat network. At the organ level, the axial skeleton acquires its first skeletal elements as neural and haemal arches, followed by chordocentra and, later, by the skeletal layers from the scleratome that sculpt

amphicoelous vertebrae and fuse centra and arches. In concert, these morphological changes underwrite changes in the mechanical function of the axial skeleton over the life cycle of salmon.

Acknowledgements

For supply of material, we wish to thank a number of farming facilities within Marine Harvest, and in particular Hans Svensvik at Tveitvågen, Askøy, Norway. Valuable material was also generously supplied by Anne Yddal, Sekkingstad AS, Sotra; Norway, Industrielaboratoriet, Bergen; Norway, and Institute of Marine Research, Matre, Norway. We are indebted to Nina Ellingsen, Department of Biology, UiB, for expert help with the histology. J.L. was supported by the National Science Foundation (USA, INSPiRE, Special Projects, grant no. 1344227).

Author contributions

Segments of the master's theses of I.R. and K.N. are included in this study. H.W. and T.K. conducted the pressure tests, and wrote the text on these. H.K. designed the study, did most of the dissections, participated in all data acquisition, made all drawings, drafted the manuscript, and contributed in all phases of manuscript production. J.L. and H.K. constructed the functional models and conducted statistical analyses. J.L., G.K.T., and P.G.F. were involved in all phases of planning, practical work and writing of the manuscript. All authors contributed to the final version of the manuscript.

Conflict of interest

The authors declare no conflict of interest.

References

- Adams DS, Keller R, Koehl MA (1990) The mechanics of notochord elongation, straightening and stiffening in the embryo of *Xenopus laevis*. *Development* **110**, 115–130.
- Bensimon-Brito A, Carreira J, Cancela L, et al. (2012) Distinct patterns of notochord mineralization in zebrafish coincide with the localization of Osteocalcin isoform 1 during early vertebral centra formation. *BMC Dev Biol* **12**, 12–28.
- Corallo D, Trapani V, Bonaldo P (2015) The notochord: structure and functions. *Cell Mol Life Sci* **72**, 2989–3008.
- Czuwala PJ, Long JH, Koob-Emunds M, et al. (2000) Hydrostatic pressure variations within the hagfish (*Myxine glutinosa*) notochord. *Bull MDI Biol Lab* **39**, 104–107.
- Ellis K, Bagwell J, Bagnat M (2013a) Notochord vacuoles are lysosome-related organelles that function in axis and spine morphogenesis. *J Cell Biol* **200**, 667–679.
- Ellis K, Hoffman BD, Bagnat M (2013b) The vacuole within. How cellular organization dictates notochord function. *Bioarchitecture* **3**, 64–68.
- Fadnes HO, Reed RK, Aukland K (1977) Interstitial fluid pressure in rats measured with a modified wick technique. *Microvasc Res* **14**, 27–36.
- Fleming A, Keynes RJ, Tannahill D (2004) A central role for the notochord in vertebral patterning. *Development* **131**, 873–880.
- Fleming A, Kishida MG, Kimmel CB, et al. (2015) Review: Building the backbone: the development and evolution of vertebral patterning. *Development* **142**, 1733–1744.
- Glickman NS, Kimmel CB, Jones MA, et al. (2003) Shaping the zebrafish notochord. *Development* **130**, 873–887.
- Grotmol S, Kryvi H, Nordvik K, et al. (2003) Notochord segmentation may lay the pathway for the development of the vertebral bodies of the Atlantic salmon *Salmo salar*. *Anat Embryol* **207**, 263–272.
- Grotmol S, Kryvi H, Nordvik K, et al. (2005) A segmental pattern of alkaline phosphatase (ALP) activity within the notochord coincides with the initial formation of the vertebral bodies. *J Anat* **206**, 427–436.
- Grotmol S, Kryvi H, Keynes R, et al. (2006) Stepwise enforcement of the notochord and its intersection with the myoseptum: an evolutionary path leading to development of the vertebra? *J Anat* **209**, 339–357.
- Hall BK (2005) *Bones and Cartilage: Developmental and Evolutionary Skeletal Biology*. London: Elsevier/Academic Press.
- Hansen TJ, Møller D (1985) Yolk absorption, yolk sac constrictions, mortality, and growth during first feeding of Atlantic salmon (*Salmo salar*) incubated on astro-turf. *Can J Fish Aquat Sci* **42**, 1073–1078.
- Holland ND, Chen J (2001) Origin and early evolution of the vertebrates: new insights from advances in molecular biology, anatomy, and palaeontology. *BioEssays* **23**, 142–151.
- Janvier P (1996) *Early Vertebrates*. Oxford: Clarendon Press.
- Kacem A, Meunier FJ, Bagliniere JL (1998) A quantitative study of morphological and histological changes in the skeleton of *Salmo salar* during its anadromous migration. *J Fish Biol* **53**, 1096–1109.
- Kaneko T, Freeha K, Wu X, et al. (2016) Role of notochord cells and sclerotome-derived cells in vertebral column development in fugu, *Takifugu rubripes*: histological and gene expression analyses. *Cell Tissue Res* **336**, 37–49.
- Koehl MAR, Adams DS, Keller RE (1990) Mechanical development of the notochord in early tail-bud amphibian embryos. In: *Biomechanics of Active Movement and Deformation of Cells* (ed. Akkas N), pp. 471–485, Berlin: Springer-Verlag.
- Koehl MAR, Quillin KJ, Pell CA (2000) Mechanical design of fibre-wound hydraulic skeletons: the stiffening and straightening of embryonic notochords. *Am Zool* **40**, 28–41.
- Koob TJ, Long JH Jr (2000) Vertebrate body axis: evolution and mechanical function. *Am Zool* **40**, 1–18.
- Kuntz YW (2004) *Developmental Biology of Teleost Fishes*. Dordrecht: Springer.
- Kvellestad A, Høie S, Thorud K, et al. (2000) Platyspondyly and shortness of vertebral column in Atlantic salmon *Salmo salar* in Norway – description and interpretation of pathologic changes. *Dis Aquat Organ* **39**, 97–108.
- Long JH Jr (1995) Morphology, mechanics, and locomotion: the relation between the notochord and swimming motions in sturgeon. *Environ Bio Fishes* **44**, 199–211.
- Long JH Jr, Koob-Emunds M, Koob TJ (1998) Does the notochord matter? Bending mechanics of hagfish (*Myxine glutinosa*). *Bull MDI Biol Lab* **37**, 114–116.
- Long JH Jr, Koob-Emunds M, Koob TJ (2004) The mechanical consequences of vertebral centra. *Zoology* **117**, 19–21.

- Long JH Jr, Engel V, Combie K, et al. (2006a) A target for biomimetics and synthetic biology: the notochord of the Atlantic hagfish, *Myxine glutinosa*. *Bull MDI Biol Lab* **45**, 78–81.
- Long JH Jr, Koob-Emunds TJ, Irving K, et al. (2006b) Biomimetic evolutionary analysis: testing the adaptive value of vertebrate tail stiffness in autonomous swimming robots. *J Exp Biol* **205**, 3819–3831.
- Long JH Jr, Krenitsky NM, Roberts SF, et al. (2011) Testing biomimetic structures in bioinspired robots: how vertebrae control the stiffness of the body and the behaviour of fish-like swimmers. *Integr Comp Biol* **51**, 158–175.
- Meijering E, Dzyubachyk O, Smal I (2012) Methods for cell and particle tracking. *Methods Enzymol* **504**, 183–200.
- Nelson JS (2006) *Fishes of the World*, 3rd edn. New York: John Wiley and Sons.
- Nordvik K, Kryvi H, Totland GK, et al. (2005) The salmon vertebral body develops through mineralization of two preformed tissues that are encompassed by two layers of bone. *J Anat* **206**, 103–114.
- Nowroozi BN, Harper CJ, de Kogel B, et al. (2012) Regional variation in morphology of vertebral centra and intervertebral joints in striped bass, *Morone saxatilis*. *J Morphol* **273**, 441–452.
- Quillin KJ (1998) Ontogenetic scaling of hydrostatic skeletons: geometric, static stress and dynamic stress scaling of the earthworm *Lumbricus terrestris*. *J Exp Biol* **201**, 1871–1883.
- Sagstad A, Grotmol S, Kryvi H, et al. (2011) Identification of vimentin- and elastin-like transcripts specifically expressed in developing notochord of Atlantic salmon (*Salmo salar* L.). *Cell Tissue Res* **346**, 191–202.
- Schmitz RJ (1995) Ultrastructure and function of cellular components of the intercentral joint in the percoid vertebral column. *J Morphol* **226**, 1–24.
- Schmitz RJ (1998) Immunohistochemical identification of the cytoskeletal elements in the notochord cells of bony fishes. *J Morphol* **236**, 105–116.
- Shi J, Keller R (1992) Cell motility driving mediolateral intercalation in explants of *Xenopus laevis*. *Development* **116**, 901–914.
- Sinwell BJ, Czuwala PJ, Long JH, et al. (1999) Bending mechanics of the hagfish (*Myxine glutinosa*) notochord under different osmotic treatments. *Bull MDI Biol Lab* **38**, 94–96.
- Stemple DL (2005) Structure and function of the notochord: an essential organ for chordate development. *Development* **132**, 2503–2512.
- Symmons S (1979) Notochordal and elastic components of the axial skeleton of fishes and their functions in locomotion. *J Zool* **189**, 157–206.
- Wang S, Kryvi H, Grotmol S, et al. (2013) Mineralization of the vertebral bodies in Atlantic salmon (*Salmo salar* L.) is initiated segmentally in the form of hydroxyapatite crystal accretions in the notochord sheath. *J Anat* **223**, 159–170.
- Wang S, Furmanek T, Kryvi H, et al. (2014) Transcriptome sequencing of Atlantic salmon (*Salmo salar* L.) notochord prior to development of the vertebrae provides clues to regulation of positional fate, chordoblast lineage and mineralisation. *BMC Genom* **15**, 141–158.
- Wiig H, Reed RK, Aukland K (1981) Micropuncture measurement of interstitial fluid pressure in rat subcutis and skeletal muscle: comparison to wick-in-needle technique. *Microvasc Res* **21**, 308–319.
- Witten PE, Gil-Martens L, Hall BK, et al. (2005) Compressed vertebrae in Atlantic salmon (*Salmo salar*). Evidence for metaplastic chondrogenesis as skeletogenic response late in ontogeny. *Dis Aquat Organ* **64**, 237–246.